

1 A Bayesian approach to explore signal execution mechanisms in programmed cell  
2 death.

3 Michael A. Kochen<sup>1</sup>, Carlos F. Lopez<sup>1,2,\*</sup>

4

5 <sup>1</sup>Department of Biomedical Informatics, Vanderbilt University, Nashville, TN

6 <sup>2</sup>Department of Biochemistry, Vanderbilt University, Nashville, TN

7

8 \*To whom correspondence should be addressed.

9 Email: [c.lopez@vanderbilt.edu](mailto:c.lopez@vanderbilt.edu)

10

11 **Abstract**

12 Mathematical models of biochemical reaction networks are central to the exploration of  
13 network dynamics and bridge the gap between experimental measurements and mechanistic  
14 interpretations. However, model parameters are often not available and sparse experimental  
15 data leads to challenges in model calibration and parameter estimation. This can in turn lead to  
16 inaccurate mechanistic interpretations of experimental data and generate poorly conceived  
17 hypotheses for experimental validation. To address this challenge, we evaluate whether a  
18 Bayesian probability-based approach can be used to qualitatively explore biochemical network  
19 execution mechanisms. To test this approach, we explore the parameter space of extrinsic  
20 apoptosis to identify the preferred mode of signal execution. Apoptosis signal processing can  
21 take place either through a mitochondria independent (Type I) mode or a mitochondria  
22 dependent (Type II) mode. We first show that model subnetworks successfully identify the  
23 most likely execution mode for a specific concentration of key molecular regulators. We then  
24 show that changes in molecular regulator concentrations alter the overall reaction flux through  
25 the network shifting modulating signal flow primarily through either a caspase-only pathway or  
26 through the mitochondria. Our work thus demonstrates that Bayesian probability approaches  
27 can be used to explore the dynamic behavior of model biochemical systems even with missing  
28 or sparse data.

29

30 **Introduction**

31 Emergent cellular behaviors from complex biochemical network processes are difficult to  
32 characterize due to the complex interplay between system components and their interactions  
33 [1, 2, 3]. Mathematical models of biochemical processes have evolved alongside experimental  
34 measurements to explain observed cellular behaviors and guide hypothesis construction for  
35 further testing [4, 5]. Models of biochemical reaction networks are typically based on the Mass-  
36 Action kinetics formalism and built to represent known pathway mechanics with knowledge  
37 garnered from years or even decades of experimentation [6, 7]. Although these models have  
38 yielded important predictions and insights about biochemical network processes, they also  
39 depend on kinetic rate parameters and protein concentrations that are often poorly  
40 characterized or simply unavailable. A typical work-around is to employ model calibration  
41 methods to estimate suitable parameters values via optimization to protein concentration  
42 time-course data, which is often scarce [8, 9, 10]. It has also been shown that vector-based  
43 methods can find multiple parameter sets whereby models agree with experimental data,  
44 based on goodness-of-fit metrics, but the dynamics of the network can exhibit significantly  
45 different execution modes [7, 9]. This poses a challenge for the study of dynamic network  
46 processes as the mode of signal execution can be highly dependent on a specific parameter set  
47 and could in turn lead to inadequate model-based interpretation. Therefore, an approach that  
48 can enable researchers to explore the execution mechanisms of a biochemical process from a  
49 probabilistic perspective, constrained only by available data, would facilitate a rigorous  
50 exploration of network dynamics and accelerate the generation of testable mechanistic  
51 hypotheses [11].

52 In this work, we explore whether a Bayesian probability approach can identify network  
53 execution modes in extrinsic apoptosis restricted only by experimental observations. Two  
54 execution modes have been identified for extrinsic apoptosis signaling: a mitochondria  
55 independent (Type I) mode, whereby initiator caspases directly activate effector caspases and  
56 induce cell death, and a mitochondria dependent (Type II) mode whereby initiator caspases  
57 engage the Bcl-2 family of proteins, which eventually lead to effector caspase activation (see  
58 Box 1 for biology details). Most mammalian cells execute apoptosis via the Type II mechanism,  
59 yet the Type I mechanism plays a central role in specific cell types, particularly certain types of  
60 lymphocytes [12]. A significant body of experimental and modeling work has identified key  
61 regulators for Type I vs Type II execution (see Box 1). However, it is still unclear how network  
62 structure and the interplay among multiple regulators can modulate signal execution for either  
63 Type I or Type II modes. A more traditional approach would prescribe intricate and detailed  
64 experimental measurements of cellular response to yield the desired data and improve our  
65 understanding of signal execution. However, the time and cost associated with such  
66 experiments makes it unlikely and at times unfeasible to obtain said data. It is here that we see  
67 Bayesian inference approaches as a complementary alternative to experimentation that can  
68 provide qualitative insights about signal execution mechanisms, by exploring broad parameter  
69 space ranges, subject only to available computer time.

71 Here we show that a Bayesian parameter exploration approach, constrained by network  
72 structure or molecular concentrations, can identify the dominant signal execution modes in a  
73 reaction network. Specifically, we demonstrate the dependence of Type I or a Type II cellular  
74 apoptosis execution on network structure and chemical-species concentrations. We use  
75 Bayesian model evidence as a metric for comparisons of signal flow through different pathways  
76 of the network and subnetworks to identify how regulators affect execution modes. We  
77 introduce two complementary approaches that can be used in tandem to explore signal  
78 execution modulation. We first define a *multimodel exploration method* to explore multiple  
79 hypothesis about apoptosis execution by deconstructing an established apoptosis network  
80 model into functional subnetworks. We also define a *pathway flux method* to characterize the  
81 signal flux through specific network pathways within the complete network. Combined, these  
82 two approaches enable us to qualitatively identify key network components and molecular  
83 regulator combinations that shed mechanistic insights about apoptosis execution. Our  
84 approach is generalizable to other mass-action kinetics-based networks where signal execution  
85 modes play important roles in cellular outcomes. The work leverages Nested Sampling  
86 algorithm methods to efficiently calculate Bayesian evidence on high performance computing  
87 (HPC) platforms, both of which are seldom used in biological applications. In this manner we  
88 are able to carry out the necessary calculations to explore parameter space and estimate the  
89 model evidence within the timespan of days.

## 90 Methods

### 91 Apoptosis model and simulations

92 The base model used in this work is a modified version of the Extrinsic Apoptosis Reaction  
93 Model (EARM) from Lopez et al. (EARM v2.1) [7]. The original EARM was simplified to reduce  
94 complexity in the number of parameters, but still retains the key features of the network for  
95 apoptosis execution. Specifically, we reduced the molecular complexity of mitochondrial outer  
96 membrane permeabilization (MOMP) down to a representative set of Bcl-2 proteins that  
97 capture the behavior of activators, inhibitors, effectors, and sensitizers. We also eliminated  
98 intermediate states for Cytochrome-c and SMAC to streamline effector caspase activation, and  
99 we added an explicit FADD molecule, a part of the death-inducing signaling complex (DISC) to  
100 achieve a more realistic representation of signal initiation. Overall, EARM v2.1 comprised 16  
101 chemical species at non-zero initial concentrations, 50 total chemical species, 62 reactions, and  
102 62 kinetic parameters. The modified model was recalibrated to recapitulate the time-  
103 dependent concentration trajectories of truncated Bid, Smac release from the mitochondria,  
104 and cleaved PARP analogous to the approach reported previously [42] (Figure S1). The modified  
105 EARM was partitioned into six sub-models, encoded in PySB, and are summarized in Figure 2.  
106 All simulations were run using the mass-action kinetics formalism as a system of Ordinary  
107 Differential Equations (ODEs) using the VODE integrator in SciPy, within the PySB modeling  
108 framework. All data results, representative models, and software are distributed with open-  
109 source licensing and can be found in the GitHub repository <https://github.com/LoLab-VU/BIND>.

110

111

112

113 **Bayesian evidence estimation**

114 Bayesian evidence is the normalizing term in a Bayesian calculation and provides a measure for  
115 model comparison with regard to their fit to experimental data. It is expressed as:

116 
$$P(D|M) = \int L(D|\theta, M) P(\theta|M) d\theta \quad (1)$$

117 Where  $M$  is the model under consideration,  $D$  is the experimental data,  $\theta$  is a specific set of  
118 parameter values,  $L(D|\theta, M)$  is the likelihood function describing the fit of the data to the  
119 model under those parameter values, and  $P(\theta|M)$  is the prior distribution of parameters. All  
120 evidence estimates were made using the nested sampling method, introduced by Skilling [43].  
121 This method simplifies the evidence calculation by introducing a prior mass element  $dX =$   
122  $P(\theta|M) d\theta$  that is estimated by  $(X_{i-1} - X_i)$  where  $X_i = e^{-i/N}$ ,  $i$  is the current iteration of the  
123 algorithm, and  $N$  is the total number of live points. The evidence is then written as

124 
$$Z = \int_0^1 L dX \approx \sum_{i=1}^1 L_i (X_{i-1} - X_i) \quad (2)$$

125 Initialization of the algorithm is carried out by randomly selecting an initial population of  
126 parameter sets (points in parameter space) from the prior distribution, scoring each one with  
127 the likelihood function, and ranking them from  $L_{high}$  to  $L_{low}$ . At each iteration of the algorithm  
128 a new set of parameter values is selected and scored. If that score is higher than  $L_{low}$ , then it is  
129 added to the population, at the appropriate rank, and  $L_{low}$  is removed from the population and  
130 added to the evidence sum (2).

131 **Nested sampling software**

132 All evidence estimates in this work are calculated with MultiNest, a nested sampling-based  
133 algorithm designed for efficient evidence calculation on highly multimodel posterior  
134 distributions [44, 45]. MultiNest works by clustering the live points (population of parameter  
135 sets) and enclosing them in ellipsoids at each iteration. The enclosed space then constitutes a  
136 reduced space of admissible parameter sets. This lowers the probability of sampling from low  
137 likelihood areas and evaluating points that will only be discarded. The evidence estimate is  
138 accompanied by an estimate of the evidence error. The algorithm terminates when the  
139 presumed contribution of the highest likelihood member of the current set of live points,  
140  $L_{high} X_i$  is below a threshold. Here, we use a threshold of 0.0001 and a population size and  
141 16,000 unless otherwise noted. See [44, 45], for more details on the MultiNest algorithm. We  
142 use MultiNest with the Python wrapper PyMultiNest [46], which facilitates the integration with  
143 PySB into the parameter sampling pipeline.

144 **Multimodel exploration analysis.**

145 To explore multiple hypotheses for signal execution under different biochemical network  
146 structures, we carried out an analysis inspired in the multi-model inference approach [47, 48].  
147 We broke down the EARM network into six subnetworks and tested each across increasing  
148 concentrations of the regulator XIAP for efficacy in achieving apoptosis. We define the  
149 proportion of cleaved PARP, relative to total PARP, as a metric for effective apoptosis  
150 execution. That is, if all PARP has been cleaved, then apoptosis has been completely achieved.  
151 We therefore define an objective function that estimates the amount of cleaved PARP as:

152 
$$Obj_{multimodel} = \frac{cParp}{tParp} \quad (3)$$

153 where  $cParp$  is the amount of PARP that has been cleaved and  $tParp$  is the total amount of  
154 PARP in the system.

155 When this objective function is substituted into equation (1) in place of the likelihood function,  
156 the evidence calculation produces an expected value, an average over the chosen prior  
157 parameter range for the proportion of PARP that has been cleaved. In this work we compare  
158 the expected values for different subnetworks, pathways, and regulatory conditions only in  
159 qualitative terms and as a relative measure of fit to an outcome represented by the objective  
160 function.

161 **Pathway flux analysis.**

162 We also explored the effect of molecular regulators of Type I vs Type II execution relative to the  
163 apoptosis signal flux through the network as we have done in previous work [49]. Briefly, signal  
164 flux is defined as the chemical reaction flux in units of molecules per unit time, that traverses  
165 through a given pathway. In the apoptosis network there are two potential pathways that can  
166 lead to Caspase-3 activation and subsequently PARP cleavage. In the direct caspase pathway  
167 initiator caspases represented here as “Caspase-8” directly cleave and activate the effector  
168 caspases represented here as “Caspase-3”. By contrast, in the mitochondrial pathway, effector  
169 caspases are activated via the apoptosome, and are dependent on mitochondrial outer  
170 membrane permeabilization (MOMP). Therefore, the dominant pathway responsible for  
171 Caspase-3 activation defines the route of the signal. To estimate the flux through the Type I vs  
172 Type II pathway, we define an objective function as:

173 
$$Obj_{pathway} = \sum_{t=0}^T \frac{\sum_0^t C3_{pathway}}{\sum_0^t C3_{total}} \times (cParp_t - cParp_{t-1}) \quad (4)$$

174 where  $t$  represents time in seconds,  $\sum_0^t C3_{pathway}$  is the amount of Caspase-3 activated via the  
175 target pathway up to time  $t$ ,  $\sum_0^t C3_{total}$  is the total Caspase-3 activated up to time  $t$ ,  
176 and  $\sum_0^t C3_{pathway} / \sum_0^t C3_{total}$  is the proportion of activated Caspase-3 that was produced via  
177 the target pathway up to time  $t$ .  $(cParp_t - cParp_{t-1})$  is the total PARP that has been cleaved,  
178 and activated, by Caspase-3 from time  $t - 1$  to time  $t$ . Thus, at any given time  $t$  we can estimate  
179 the amount of Caspase-3 that has been activated through a specific pathway. Multiplication of  
180 these two terms returns an estimate for the amount of PARP cleaved via the specific pathway  
181 at time  $t$ . Summing over  $T$  then returns an estimate for the total apoptosis signal flowing  
182 through the target pathway. Like the PARP cleavage objective function, the signal flux objective  
183 substituted into equation (1) produces an estimate of the average flux over a defined prior  
184 distribution. We estimated this quantity over increasing concentrations of the of the molecular  
185 regulator XIAP, but also at high and low levels of the DISC components FADD and Caspase-8.  
186 The total signal flux was estimated by summing the evidence estimates for the flux through  
187 either the direct caspase or mitochondrial pathway.

188 **Parameter ranges and initial conditions.**

189 The prior distribution takes the form of a set of parameter ranges, one for each reaction rate  
190 parameter. The chosen ranges span four orders of magnitude around generic reaction rates

191 deemed plausible [4] and are specific to the type of reaction taking place. The ranges of  
192 reaction rate parameters, in  $\text{Log}_{10}$  space, are 1<sup>st</sup> order forward: [-4.0, 0.0], 2<sup>nd</sup> order forward: [-  
193 8.0, -4.0], 1<sup>st</sup> order reverse: [-4.0, 0.0], catalysis: [-1.0, 3.0]. These ranges were also used in  
194 calibration of the base model. Initial conditions were either gleaned from the literature [50, 51]  
195 or taken from a previous model of extrinsic apoptosis [7]. Because the baseline model was  
196 designed to concur with Type II apoptotic data (see above), literature derived initial conditions  
197 were based on Type II Jurkat or Hela cell lines (Table S1).

198 **Bayes factors.**

199 Evidence estimates are often used to select between two competing models by calculating the  
200 Bayes factor (i.e. the ratio of their evidence values). This provides a measure of confidence for  
201 choosing one model over another. We can likewise use trends in evidence values to produce  
202 trends in Bayes factors that provide additional insights into the dynamical relationship between  
203 pathways. To facilitate construction of Bayes factor trends with a continuous and symmetric  
204 range, the we calculated Bayes factors as:

$$205 \quad Bf = \begin{cases} -\frac{Z_2}{Z_1} + 1 & \text{if } Z_1 < Z_2 \\ \frac{Z_1}{Z_2} - 1 & \text{if } Z_1 > Z_2 \end{cases}$$

206 where  $Z_1$  and  $Z_2$  are the evidence estimates for two pathways under comparison.

207 **Computational resources**

208 Because of the high computational workload necessary for this analysis, a wide range of  
209 computational resources were used. The bulk of the work was done on the ACCRE cluster at  
210 Vanderbilt University which has more than 600 compute nodes running Intel Xeon processors  
211 and a Linux OS. As many as 300 evidence estimates were run in parallel on this system.  
212 Additional resources included two local servers, also running Intel processors and a Linux OS, as  
213 well as a small local four node cluster running Linux and AMD Ryzen 1700 processors. A  
214 detailed breakdown of CPU time can be found in the results section. In all evidence estimates  
215 for 14 different networks/initial conditions were made across the range of XIAP concentrations.  
216 We estimate all 14 runs would take ~9 days each on a typical university server with 32 cores/64  
217 threads.

218

219

220

221

222

223

224

## 225 Results

### 226 Overview: A Bayesian evidence approach to explore mechanistic hypotheses.

227 Our overarching goal is to understand the mechanisms and dynamics of biochemical networks  
228 responsible for cellular commitment to fate, given incomplete or unavailable data. We take a  
229 Bayesian probability approach to study model subnetworks and specific model pathways as  
230 summarized schematically in Figure 1 to estimate the evidence for signaling execution  
231 mechanisms given a set of experimental data and existing priors.

232 In the *Multimodel Exploration Analysis* (Figure 1, left path), the network model is deconstructed  
233 into biologically relevant subnetworks and the probability of each subnetwork achieving  
234 apoptosis, under various regulatory conditions, is estimated via Bayesian evidence. This differs  
235 from traditional model selection and multimodel inference applications where models are  
236 typically ranked based on their fit to experimental data and high-ranking models may be  
237 averaged to obtain a composite model [47, 48, 52, 53, 54, 55]. Here, we already have a model  
238 that captures key features of programmed cell death execution. Instead, we use the  
239 differences in evidence to construct a composite picture of mechanistic evidence for apoptosis  
240 execution. To achieve this, we first tailor the objective function to represent signal execution  
241 strength, as measured by cleaved PARP concentration at the end of the simulation. The  
242 evidence derived from this objective function therefore describes the likelihood that the signal  
243 is effectively transmitted through the (sub)network. It should be noted that Bayesian evidence  
244 inherently incorporates model complexity as the objectives are integrated over normalized  
245 prior distributions [44, 52, 56]. As we will see, comparison of changes in signal strength through  
246 relevant subnetworks allows inferences to be made on the effect of the perturbed network  
247 regulator as well as various network components on the overall dynamics of the system. We  
248 focus primarily on understanding how Bayesian evidence for the caspase pathway compares to  
249 that of the complete network as these are most relevant for the analysis of Type I/II execution  
250 modes. This analysis will inform on how network components contribute to overall signal  
251 execution and provide mechanistic insights about the sensitivity of PARP cleavage to  
252 subnetwork components.

253 In the *Pathway Flux Analysis* (Figure 1, right path), we retain the complete network structure  
254 but instead tailor the objective functions to measure biochemical reaction flux, as described in  
255 the Methods section, through either the direct caspase or mitochondrial pathways. We  
256 primarily consider the influence of the apoptosis inhibitor XIAP on regulatory dynamics and  
257 phenotypic fate but also consider the regulatory effect of the death inducing signaling complex  
258 (DISC) and the anti-apoptotic protein Bcl-2, all of which have been found to be relevant to Type  
259 I vs Type II execution in different cell types [13, 14]. This analysis will inform on how molecular  
260 regulators modulate biochemical flux through the network and their influence on apoptosis  
261 completion as measured by PARP cleavage.

### 262 Decomposition of the extrinsic apoptosis network and reductive analysis of the effects of 263 XIAP

264 To investigate the effect of network substructures on apoptosis signaling, we build a composite  
265 description of system dynamics by observing variations in signal throughput, represented by  
266 evidence values for PARP cleavage, between subnetworks (Figure 2A-F) relative to changes in

267 regulatory conditions. We consider relative changes in the evidence values as the number of  
268 XIAP molecules is increased where a higher evidence value indicates a stronger signal over the  
269 prior range of parameter values. XIAP was varied from 0 to 200,000 molecules per cell in  
270 increments of 250 to explore how changes in XIAP affect the likelihood of apoptosis execution.  
271 For subnetworks that include the mitochondrial pathway, Bcl-2 (an anti-apoptotic) was reduced  
272 or eliminated, to explore Type I vs Type II activity independent of inhibitors that could confound  
273 signal throughput, and more closely simulate a cells that is “primed” for death [56]. All other  
274 initial values were fixed at the levels shown in supplementary Table S1. In the absence of XIAP  
275 all six subnetworks have evidence estimates greater than 0.98, (Figure 2 A: 0.993, B: 0.998, C:  
276 0.992, D: 0.981, E: 0.998, F: 0.981, Table S2) indicating that they can all capture a biological  
277 process that leads to PARP cleavage across the allowed range of parameters, as expected. We  
278 further explore how XIAP can modulate Type I/II apoptosis execution for a chosen subnetwork .  
279 The results in Jost et al. [14] imply that the cellular level of XIAP determines the preferred  
280 apoptosis pathway with higher levels specific to Type II cells and lower levels specific to Type I.  
281 To hypothesize a possible mechanistic explanation for this behavior we compared the  
282 computed the Bayesian evidence values, over increasing concentrations of XIAP, for the direct  
283 caspase activation network against both the complete network and the mitochondrial network  
284 (Figures 2A and G green; 2E and G orange; 2F G blue respectively). . This mimics reported  
285 experimental strategies to study Type I/II phenotypes and allows us to gauge the effect of XIAP  
286 on networks with and without a mitochondrial component [13, 35].  
287 As XIAP levels increase we see differential effects on all subnetworks in the form of diverging  
288 evidence estimates, indicating differences in the efficacy of XIAP induced apoptotic inhibition.  
289 The evidence values for the isolated caspase pathway (Figure 2G green) diverges from the  
290 complete network (Figure 2G orange) and mitochondrial pathway (Figure 2 blue) showing a  
291 steeper initial decline that diminishes as XIAP continues to increase. PARP cleavage evidence  
292 values for the caspase pathway falls to 0.5 at an XIAP level of roughly 32,000. However, the  
293 complete network and mitochondrial pathways require XIAP levels nearly threefold higher with  
294 the evidence value reaching 0.5 at around 92,000 and 95,000 respectively.  
295 Because the direct caspase activation pathway (Figures 2G green) is representative of the Type I  
296 phenotype, the disproportionate drop in its evidence of PARP cleavage as XIAP concentration  
297 increases is consistent with experimental evidence showing XIAP-induced transition from a  
298 Type I to a Type II execution mode [14]. The complete network, containing the full  
299 mitochondrial subnetwork, and mitochondrial only pathway are also affected by XIAP but  
300 exhibits resistance to its anti-apoptotic effects, a difference that is most prominent at  
301 moderate levels of the inhibitor. This suggests a growing dependence on mitochondrial  
302 amplification for effective apoptosis as XIAP increases from low to moderate levels. At higher  
303 levels of XIAP the evidence values for the caspase pathway level off and the gap between it and  
304 the two mitochondrial containing networks narrows. The disproportionate effect of XIAP  
305 inhibition of apoptosis on the caspase pathway suggests that the mechanism for XIAP induced  
306 transition to a Type II pathway can be attributed to differential inhibition of the apoptotic signal  
307 through the isolated caspase pathway vs a network with mitochondrial involvement.

308 We note here that the small differences in evidence values between the various networks  
309 should not be surprising since every subnetwork being considered is capable of carrying  
310 apoptosis to completion, as measured by PARP cleavage. Thus, we should not expect evidence  
311 differences that would rule out any model under a model selection criterion. The log-evidence  
312 version of Figure 2G along with estimated errors generated by MultiNest are displayed in Figure  
313 S2.

314 The next two highest trends in evidence values after that of the direct caspase network (Figure  
315 2G green) belong to the networks representing direct caspase activation plus mitochondrial  
316 activation and mitochondrial activation alone (Figures 2G purple and 2G brown). For most of  
317 the range with XIAP below 100,000 these two networks have largely overlapping evidence  
318 trajectories, despite the fact that the former has twice as many paths carrying the apoptotic  
319 signal. Near an XIAP level of 100,000 the two trends diverge as the decrease in evidence values  
320 for the mitochondrial activation only network accelerates. This could be explained by XIAP  
321 overwhelming the Apoptosome at these higher levels. The apoptosome is an apoptosis inducing  
322 complex (via Caspase-3 cleavage) consisting of Cytochrome C, APAF-1, and Caspase-9, and is an  
323 inhibitory target of XIAP. As XIAP increases past 125,000 the mitochondrial activation only  
324 evidence values fall below even the solo direct caspase values, possibly due to the two-pronged  
325 inhibitory action of XIAP at both the Apoptosome and Caspase-3. An interesting observation  
326 here is that the addition of the direct caspase pathway to the mitochondrial activation pathway  
327 does not appear to increase the likelihood of achieving apoptosis for lower values of XIAP.

328 Evidence values for the network representing direct caspase activation plus mitochondrial  
329 inhibition of XIAP are in red in Figure 2G. Below an XIAP level of 100,000 these values are  
330 consistently above the evidence values for the network of the direct caspase plus mitochondrial  
331 activation. Note that while direct caspase activation does not appear to increase the likelihood  
332 of achieving apoptosis when added to the mitochondrial activation pathway (Figure 2G purple)  
333 the amplification of the direct caspase activation via mitochondrial inhibition of XIAP leads to a  
334 higher likelihood than solo activation through the mitochondria. This suggests the possibility  
335 that the primary mechanism for mitochondrial apoptotic signal amplification, under some  
336 conditions, may be inhibition of XIAP, with direct signal transduction a secondary mechanism.  
337 Above an XIAP level of 100,000, the direct caspase with XIAP inhibition values drop to levels  
338 roughly in line with the values for direct caspase activation plus mitochondrial activation,  
339 possibly due to the fact that Smac, the mitochondrial export that inhibits XIAP, is also set to  
340 100,000 molecules per cell. Both, however, remain more likely to attain apoptosis than direct  
341 caspase activation alone.

342 The two subnetworks with the highest evidence values for apoptotic signal execution are the  
343 complete network and the isolated mitochondrial pathway (Figures 2E orange and 2F blue). As  
344 previously mentioned, both of these networks contain the full mitochondrial pathway implying  
345 that this pathway supports resistance to XIAP inhibition of apoptosis. Between XIAP levels of 0  
346 to 100,000 the two trends track very closely, with the mitochondrial only pathway showing a  
347 slight but consistent advantage for apoptosis execution. The average difference between an  
348 XIAP level of 20,000 and 80,000 is roughly 0.014, meaning we expect the average PARP  
349 cleavage to favor the mitochondrial only pathway by about 1.4 percentage points, which may  
350 seem unremarkable. Context matters however, and the context here is that the complete

351 network has potentially twice the bandwidth for the apoptotic signal, namely the addition of  
352 the more direct caspase pathway. Together, this raises the possibility that under some  
353 conditions the caspase pathway is not a pathway but a sink for the apoptotic signal. In such a  
354 scenario, the signal through the caspase pathway would get lost as Caspase-3 is degraded by  
355 XIAP. Not until the signal through the mitochondrial pathway begins inhibiting XIAP could the  
356 signal proceed. Around the 100,000 level of XIAP the evidence trend for the mitochondrial  
357 pathway crosses below that for the complete network. This could be due to the parity with  
358 Smac, components of the Apoptosome, or a combination of the two.

359 **Apoptosis signal strength drives signal route through the network**

360 The results in Scaffidi et al. [13] indicate a strong phenotypic dependence on the strength of the  
361 apoptosis signal. Here we examine hypotheses made in that work and the interplay between  
362 the DISC and XIAP regulatory axes. We once again increase XIAP from 0 to 200,000 molecules  
363 in increments of 250, but this time at a low number of DISC complexes by lowering the initial  
364 values of both the scaffold protein FADD and the initiator Caspase-8, from 130,000 to 100  
365 molecules per cell. In addition to the Multimodel Exploration Approach used in the previous  
366 section, we also use the Pathway Flux Approach using the flux objective function (see  
367 Methods). In this way we attain a holistic view of network dynamics that incorporates both,  
368 network structure and flux cross-talk from all possible pathways. Additional analysis of caspase  
369 and mitochondrial pathway signal flux over a range of values for both XIAP and BCL-2 is  
370 displayed in Figure S3 and interpreted in Text S1.

371 Figure 3A displays the PARP cleavage evidence values along with their low DISC counterparts.  
372 Two things are immediately apparent. The PARP cleavage evidence values for the caspase  
373 pathway at low number of DISC is lower across the entire range of changes in the number of  
374 XIAP molecules. The complete network on the other hand shows almost no difference in low  
375 DISC conditions at lower values of XIAP. This supports the hypothesis that mitochondrial  
376 involvement is necessary to overcome weak DISC formation and that low number of DISC likely  
377 constitutes a Type II trait [13].

378 Figures 3B and 3C show evidence values for flux through the caspase pathway and complete  
379 network for high and low number of DISC, respectively. At higher DISC values, signal flux  
380 through the caspase pathway is consistently higher than the flux through the mitochondrial  
381 pathway. At lower DISC values the signal flux through the mitochondrial pathway exceeds the  
382 flux through the caspase pathway. Our results shed interesting mechanistic observations in the  
383 context of a previously proposed hypothesis stating that mitochondrial activation is  
384 downstream of caspase activation in Type I cells and upstream in Type II cells. If a weaker initial  
385 apoptosis cue does indeed push the signal through the mitochondrial pathway the initial  
386 activation of Caspase-8 would be weak and the amplifying activity of the mitochondria would  
387 ramp up the signal before Caspase-8 could directly activate Caspase-3. On the other hand,  
388 strong initial activation that pushes the signal through the caspase pathway would have the  
389 opposite effect. Also notable is the nearly identical trajectories of the total signal flux through  
390 the low and high DISC models. The average difference over the range of XIAP was only 0.011  
391 (Table S3). This is consistent with observations that both Type I and Type II cells respond equally  
392 well to receptor mediated apoptosis.[13]

393 Overall these results set up three mechanistic explanations for apoptosis execution. On one  
394 end, high DISC formation and low XIAP results in the independence of apoptosis from the  
395 mitochondrial pathway. This behavior is consistent with Type I cells like the SKW6.4 cell lines  
396 [13]. On the other end of the spectrum is the case with low DISC formation (and by construction  
397 low Caspase-8 activity) and near complete dependence on the mitochondrial pathway. Such  
398 behavior is consistent with Type II cells like Jurkat [13]. In between these two extremes is the  
399 case where DISC formation, and subsequent Caspase-8 activation, is high but apoptosis is still  
400 dependent on mitochondrial activity. Such behavior is consistent with MCF-7 cell that are  
401 known to have traits of both phenotypes [13].

#### 402 **Bayes factor trends and XIAP influence on Type I/II apoptosis phenotype**

403 Model selection methods typically calculate the evidence ratios, or Bayes factors to choose a  
404 preferred model and estimate the confidence of that choice [58, 59]. When comparing the  
405 changes in the evidence of an outcome as regulatory conditions change, the changes in the  
406 evidence ratios can provide additional information about changing network dynamics under  
407 regulatory perturbations. To characterize the effect of XIAP on the choice of apoptotic  
408 phenotype, Type I or II, we calculated the evidence ratios (Figure 4A), for each value of XIAP  
409 between the caspase pathway and both the complete network and mitochondrial pathway  
410 with a fully active mitochondrial pathway. In these calculations, the denominator represents  
411 the caspase pathway so that higher values favor a need for mitochondrial involvement. An  
412 interesting feature of both the complete and mitochondrial evidence ratio trends is the peak  
413 and reversal at a moderate level XIAP (Figure 4B). This reflects the initially successful inhibition  
414 of the caspase pathway that decelerates relatively quickly as XIAP increases, and a steadier rate  
415 of increased inhibition on networks that incorporate the mitochondrial pathway. The ratios  
416 peak between 45,000 and 50,000 molecules of XIAP (more than double the value of its target  
417 molecule Caspase-3 at 21,000) and represent the optimal level of XIAP for the requirement of  
418 the mitochondrial pathway and attainment of a Type II execution. Given the near monotonic  
419 decline of the evidence trends of both pathways, representing increasing suppression of  
420 apoptosis, the peak and decline in the evidence ratios could represent a shift toward complete  
421 apoptotic resistance. Our results therefore complement the observations in Aldridge et al.  
422 where a similar outcome was observed experimentally [60].

423 A common technique to study apoptosis is to knockdown Bid, overexpress Bcl-2, or otherwise  
424 shut down MOMP induced apoptosis through mitochondrial regulation. This strategy was used  
425 in Jost et al. [14] to study the role of XIAP in apoptosis and in the work of Aldridge et al. to  
426 explore Type I vs Type II execution in different cell lines [59]. Taking a similar approach, we set  
427 Bcl-2 levels to 328,000 molecules per cell, in line with experimental findings [47], to suppress  
428 MOMP activity and recreated the evidence and ratios landscapes (Figures 4C and 4D, Table S5).  
429 Under these conditions the evidence trend for the mitochondrial pathway drops well below  
430 that of the caspase pathway, which is reflected in the Bayes factor trend as a shift into negative  
431 values and indicating that the caspase pathway is favored. The evidence trend for the complete  
432 network under MOMP inhibition is shifted closer to that for the caspase pathway at higher  
433 concentrations of XIAP but the Type II pathway continues to dominate throughout the full  
434 range of XIAP. The peak for the associated Bayes factor trend is flattened as the number of XIAP  
435 increases, suggesting that increasing XIAP levels are less likely to induce a transition to a Type II

436 phenotype in a system with an already hampered mitochondrial pathway. We note that  
437 complete inhibition of MOMP would result in uninformative mitochondrial pathway evidence  
438 values. The evidence trend for the complete network would be indistinguishable from that for  
439 the caspase pathway alone and the complete/caspase ratio trend would simply flatline.  
440 However, our analysis shows that isolation of active biologically relevant subnetworks and  
441 direct comparison under changing molecular regulator conditions using trends in Bayesian  
442 evidence enables the extraction of information regarding the pathway interactions and  
443 differential network dynamics.

444 **Precision vs computational cost**

445 Increasing the precision of the evidence estimates, and tightening the evidence trendlines, is  
446 accomplished by increasing the number of live points in the nested sampling algorithm. The  
447 trade-off is an increase in the number of evaluations required to reach the termination of the  
448 algorithm and an accompanying increase in total computation time. Figures 5A and 5B display  
449 the required number of evaluations for the caspase pathway and complete network at  
450 population sizes of 500, 1000, 2000, 4000, 8000, and 16,000, when run with the PARP cleavage  
451 objective function. For both models the number of evaluations roughly doubles for every  
452 doubling in population size. Of note here is the higher number of required evaluations for the  
453 lower parameter model. The caspase pathway has only 22 parameters and required an average  
454 of 64,612 evaluations at a population size of 16,000 while the complete network, with its 56  
455 parameters required only 53,652 evaluations, on average (Table S6). Figures 5C and 5D are the  
456 average estimated errors calculated by the MultiNest algorithm over each population size for  
457 the caspase and complete networks respectively. As expected, error estimates fall roughly as  
458  $n^{-1/2}$  [61], signifying clear diminishing returns as the number of live points is increased. The  
459 average CPU process times, as estimated by Python's `time.clock()` method, are given in  
460 Figures 5E and 5F for the caspase and complete networks respectively. Despite the greater  
461 number of required evaluations for the caspase network the average clock times for the  
462 complete network is significantly higher. At a population of 16,000 the caspase network had an  
463 average clock time of 11,964 seconds compared to 76,981 for the complete network. The  
464 difference is due to the greater simulation time for the much larger complete model.  
465 Ultimately, the choice of population size for the methods we have laid out here will depend on  
466 the networks to be compared, the objective function, and how well the evidence trends must  
467 be resolved in order to make inferences about network dynamics. For example, at a population  
468 size of 500 the evidence trend for the caspase pathway is clearly discernable from the  
469 mitochondrial pathway and the complete network, but the latter two are largely overlapping  
470 (Figure S4A). At higher population levels, however, two distinct mitochondrial and complete  
471 trends become apparent (Figure S5). If Bayes factor trends are desired then the choice of  
472 population size must take into consideration the amplification of the noise from both trends  
473 (see Figures S4(B, D, F, H, J, L) for complete/caspase Bayes factor trends).

474

475

476 **Discussion**

477 Characterizing information flow in biological networks, the interactions between various  
478 pathways or network components, and shifts in phenotype upon regulatory perturbations is  
479 standing challenge in molecular biology. Although comparative analysis of signal flow within a  
480 network is possible with current computational methods, the dependence of physicochemical  
481 models on unknown parameters makes the computational examination of each network  
482 component highly dependent on costly experimentation.

483 To take advantage of the enormous amount of existing knowledge encoded in these  
484 physicochemical networks without the dependence on explicit parameter values we take a  
485 probabilistic approach to the exploration of changes in network dynamics. By integrating an  
486 objective function that represents a simulated outcome over parameter distributions we obtain  
487 the likelihood of attaining that outcome given the available information about the signaling  
488 pathways. Qualitative exploration of network behavior for various in silico experimental setups  
489 and regulatory conditions are then attainable without explicit knowledge of every parameter  
490 value. We demonstrate the utility of the method when applied to the regulation of extrinsic  
491 apoptosis. Networks that incorporate an active mitochondrial pathway displayed a higher  
492 resistance to apoptotic inhibition from increasing levels of XIAP, consistent with experimental  
493 evidence that XIAP induces a Type II phenotype [14]. Also in line with experimental evidence  
494 [13] are the results that suggest low/high signal initiation is consistent with Type II/I phenotype  
495 respectively and that both types achieve apoptosis equally well.

496 A potential limitation of a Bayesian approach to study network dynamics could be the  
497 computational cost. A number of factors affect the run time of the algorithm including size of  
498 the model, the objective function, and the desired precision. Fortunately, reducing the  
499 resolution (the number of sets of initial values for which an evidence value is estimated) and  
500 the precision (the population size) can drastically reduce the cost and in many cases the  
501 method will still be viable. One aspect of the method that is severely restrictive is the number  
502 of model components that can be varied in the same run since the computational cost  
503 increases exponentially with each additional variable. Reasonable parameter ranges must also  
504 be chosen. Information regarding the parameters can be incorporated into the evidence  
505 calculations by adjusting the range and shape of the priors. Here we used generic but  
506 biologically plausible ranges with uniform distributions and produced results that were  
507 qualitatively consistent with previous experimental results. We note, however, that our results  
508 make mechanistic inferences from model experiments given existing data over a period of  
509 weeks rather than the months or years that would be required to attain this information with  
510 experimental approaches. Our results therefore support Bayesian approaches as a suitable  
511 complement to experimentation and a shift from purely deterministic models with a single  
512 optimum parameter set to a probabilistic understanding of mechanistic models of cellular  
513 processes.

514

515

516 **Conclusions**

517 In this paper we have developed a probabilistic approach to the qualitative analysis of the  
518 network dynamics of physicochemical models. It is designed to incorporate all available  
519 knowledge of the reaction topology, and the parameters on that topology, and calculate the  
520 likelihood of achieving an outcome of interest. Inferences on network dynamics are then made  
521 by repeating this calculation under changing regulatory conditions and various *in silico*  
522 experiments. We tested the method against a model of the extrinsic apoptosis system and  
523 produced results that were consistent with several lines of experimental research. To our  
524 knowledge this is the first attempt at a probabilistic analysis of network dynamics for  
525 physicochemical models. We believe this method will prove valuable for the large-scale  
526 exploration of those dynamics, particularly when parameter knowledge and data are scarce.

527

528 **Acknowledgements**

529 This work was supported by the NIH NCI U01CA215845 (CFL), as well as NSF MCB 1411482 (CFL).  
530 We thank the Incyte-Vanderbilt Alliance (CFL) for their support of this project. We also thank  
531 the Advanced Computing Center for Research and Education (ACCRE) for computational  
532 resources and support needed to complete this work. Finally, we extend our thanks to Dr Blake  
533 Wilson for his effort in reviewing this work and providing feedback.

534

535 **References**

- 536 1. Bhalla US, Iyengar R. Emergent Properties of Networks of Biological Signaling Pathways.  
537 Science. 1999 Jan 15;283(5400):381–7.
- 538 2. Loscalzo J, Barabasi A-L. Systems biology and the future of medicine. Wiley  
539 Interdisciplinary Reviews: Systems Biology and Medicine. 2011;3(6):619–27.
- 540 3. Kitano H. Computational systems biology. Nature. 2002 Nov;420(6912):206–10.
- 541 4. Aldridge BB, Burke JM, Lauffenburger DA, Sorger PK. Physicochemical modelling of cell  
542 signalling pathways. Nat Cell Biol. 2006 Nov;8(11):1195–203.
- 543 5. Le Novère N. Quantitative and logic modelling of molecular and gene networks. Nature  
544 Reviews Genetics. 2015 Mar;16(3):146–58.
- 545 6. Albeck JG, Burke JM, Spencer SL, Lauffenburger DA, Sorger PK. Modeling a Snap-Action,  
546 Variable-Delay Switch Controlling Extrinsic Cell Death. PLOS Biology. 2008 Dec  
547 2;6(12):e299.
- 548 7. Lopez CF, Muhlich JL, Bachman JA, Sorger PK. Programming biological models in Python  
549 using PySB. Molecular Systems Biology. 2013 Jan 1;9(1):646.
- 550 8. Riel V, A.w N. Dynamic modelling and analysis of biochemical networks: mechanism-  
551 based models and model-based experiments. Brief Bioinform. 2006 Dec 1;7(4):364–74.
- 552 9. Shockley EM, Vrugt JA, Lopez CF. PyDREAM: high-dimensional parameter inference for  
553 biological models in python. Bioinformatics. 2018 Feb 15;34(4):695–7.
- 554 10. Mitra ED, Suderman R, Colvin J, Ionkov A, Hu A, Sauro HM, et al. PyBioNetFit and the  
555 Biological Property Specification Language. arXiv:190307750 [q-bio] [Internet]. 2019 Mar  
556 18 [cited 2019 Nov 1]; Available from: <http://arxiv.org/abs/1903.07750>
- 557 11. Wrede F, Hellander A. Smart computational exploration of stochastic gene regulatory  
558 network models using human-in-the-loop semi-supervised learning. bioRxiv. 2018 Dec  
559 8;490623.
- 560 12. Scaffidi C, Schmitz I, Zha J, Korsmeyer SJ, Krammer PH, Peter ME. Differential Modulation  
561 of Apoptosis Sensitivity in CD95 Type I and Type II Cells. J Biol Chem. 1999 Aug  
562 6;274(32):22532–8.
- 563 13. Scaffidi C, Fulda S, Srinivasan A, Friesen C, Li F, Tomaselli KJ, et al. Two CD95 (APO-1/Fas)  
564 signaling pathways. The EMBO Journal. 1998 Mar 16;17(6):1675–87.
- 565 14. Jost PJ, Grabow S, Gray D, McKenzie MD, Nachbur U, Huang DCS, et al. XIAP discriminates  
566 between type I and type II FAS-induced apoptosis. Nature. 2009 Aug;460(7258):1035–9.

567 15. Ashkenazi A, Dixit VM. Death Receptors: Signaling and Modulation. *Science*. 1998 Aug  
568 28;281(5381):1305–8.

569 16. Boldin MP, Varfolomeev EE, Pancer Z, Mett IL, Camonis JH, Wallach D. A Novel Protein  
570 That Interacts with the Death Domain of Fas/APO1 Contains a Sequence Motif Related to  
571 the Death Domain. *J Biol Chem*. 1995 Apr 7;270(14):7795–8.

572 17. Kischkel FC, Lawrence DA, Chuntharapai A, Schow P, Kim KJ, Ashkenazi A. Apo2L/TRAIL-  
573 Dependent Recruitment of Endogenous FADD and Caspase-8 to Death Receptors 4 and 5.  
574 *Immunity*. 2000 Jun 1;12(6):611–20.

575 18. Sprick MR, Weigand MA, Rieser E, Rauch CT, Juo P, Blenis J, et al. FADD/MORT1 and  
576 Caspase-8 Are Recruited to TRAIL Receptors 1 and 2 and Are Essential for Apoptosis  
577 Mediated by TRAIL Receptor 2. *Immunity*. 2000 Jun 1;12(6):599–609.

578 19. Krueger A, Schmitz I, Baumann S, Krammer PH, Kirchhoff S. Cellular FLICE-inhibitory  
579 Protein Splice Variants Inhibit Different Steps of Caspase-8 Activation at the CD95 Death-  
580 inducing Signaling Complex. *J Biol Chem*. 2001 Jun 8;276(23):20633–40.

581 20. Salvesen GS, Dixit VM. Caspase activation: The induced-proximity model. *PNAS*. 1999 Sep  
582 28;96(20):10964–7.

583 21. Martin DA, Siegel RM, Zheng L, Lenardo MJ. Membrane Oligomerization and Cleavage  
584 Activates the Caspase-8 (FLICE/MACH $\alpha$ 1) Death Signal. *J Biol Chem*. 1998 Feb  
585 20;273(8):4345–9.

586 22. Boatright KM, Salvesen GS. Mechanisms of caspase activation. *Current Opinion in Cell  
587 Biology*. 2003 Dec 1;15(6):725–31.

588 23. Stennicke HR, Jürgensmeier JM, Shin H, Deveraux Q, Wolf BB, Yang X, et al. Pro-caspase-3  
589 Is a Major Physiologic Target of Caspase-8. *J Biol Chem*. 1998 Oct 16;273(42):27084–90.

590 24. Li H, Zhu H, Xu C, Yuan J. Cleavage of BID by Caspase 8 Mediates the Mitochondrial  
591 Damage in the Fas Pathway of Apoptosis. *Cell*. 1998 Aug 21;94(4):491–501.

592 25. Luo X, Budihardjo I, Zou H, Slaughter C, Wang X. Bid, a Bcl2 Interacting Protein, Mediates  
593 Cytochrome c Release from Mitochondria in Response to Activation of Cell Surface Death  
594 Receptors. *Cell*. 1998 Aug 21;94(4):481–90.

595 26. Desagher S, Osen-Sand A, Nichols A, Eskes R, Montessuit S, Lauper S, et al. Bid-induced  
596 Conformational Change of Bax Is Responsible for Mitochondrial Cytochrome c Release  
597 during Apoptosis. *The Journal of Cell Biology*. 1999 Mar 8;144(5):891–901.

598 27. Kelekar A, Thompson CB. Bcl-2-family proteins: the role of the BH3 domain in apoptosis.  
599 *Trends in Cell Biology*. 1998 Aug 1;8(8):324–30.

600 28. Oltval ZN, Milliman CL, Korsmeyer SJ. Bcl-2 heterodimerizes in vivo with a conserved  
601 homolog, Bax, that accelerates programed cell death. *Cell*. 1993 Aug 27;74(4):609–19.

602 29. Leber B, Lin J, Andrews DW. Embedded together: The life and death consequences of  
603 interaction of the Bcl-2 family with membranes. *Apoptosis*. 2007 May 1;12(5):897–911.

604 30. Letai A, Bassik MC, Walensky LD, Sorcinelli MD, Weiler S, Korsmeyer SJ. Distinct BH3  
605 domains either sensitize or activate mitochondrial apoptosis, serving as prototype cancer  
606 therapeutics. *Cancer Cell*. 2002 Sep 1;2(3):183–92.

607 31. Yang E, Zha J, Jockel J, Boise LH, Thompson CB, Korsmeyer SJ. Bad, a heterodimeric  
608 partner for Bcl-xL and Bcl-2, displaces bax and promotes cell death. *Cell*. 1995 Jan  
609 27;80(2):285–91.

610 32. Kale J, Osterlund EJ, Andrews DW. BCL-2 family proteins: changing partners in the dance  
611 towards death. *Cell Death Differ*. 2018 Jan;25(1):65–80.

612 33. Tewari M, Quan LT, O'Rourke K, Desnoyers S, Zeng Z, Beidler DR, et al. Yama/CPP32 $\beta$ , a  
613 mammalian homolog of CED-3, is a CrmA-inhibitable protease that cleaves the death  
614 substrate poly(ADP-ribose) polymerase. *Cell*. 1995 Jun 2;81(5):801–9.

615 34. Nicholson DW, Ali A, Thornberry NA, Vaillancourt JP, Ding CK, Gallant M, et al.  
616 Identification and inhibition of the ICE/CED-3 protease necessary for mammalian  
617 apoptosis. *Nature*. 1995 Jul;376(6535):37–43.

618 35. Jost PJ, Grabow S, Gray D, McKenzie MD, Nachbur U, Huang DCS, et al. XIAP discriminates  
619 between type I and type II FAS-induced apoptosis. *Nature*. 2009 Aug;460(7258):1035–9.

620 36. Huang Y, Park YC, Rich RL, Segal D, Myszka DG, Wu H. Structural Basis of Caspase  
621 Inhibition by XIAP: Differential Roles of the Linker versus the BIR Domain. *Cell*. 2001 Mar  
622 9;104(5):781–90.

623 37. Suzuki Y, Nakabayashi Y, Takahashi R. Ubiquitin-protein ligase activity of X-linked  
624 inhibitor of apoptosis protein promotes proteasomal degradation of caspase-3 and  
625 enhances its anti-apoptotic effect in Fas-induced cell death. *PNAS*. 2001 Jul  
626 17;98(15):8662–7.

627 38. Shiozaki EN, Chai J, Rigotti DJ, Riedl SJ, Li P, Srinivasula SM, et al. Mechanism of XIAP-  
628 Mediated Inhibition of Caspase-9. *Molecular Cell*. 2003 Feb 1;11(2):519–27.

629 39. Zou H, Li Y, Liu X, Wang X. An APAF-1-Cytochrome c Multimeric Complex Is a Functional  
630 Apoptosome That Activates Procaspsase-9. *J Biol Chem*. 1999 Apr 23;274(17):11549–56.

631 40. Adrain C, Creagh EM, Martin SJ. Apoptosis-associated release of Smac/DIABLO from  
632 mitochondria requires active caspases and is blocked by Bcl-2. *The EMBO Journal*. 2001  
633 Dec 3;20(23):6627–36.

634 41. Cowling V, Downward J. Caspase-6 is the direct activator of caspase-8 in the cytochrome  
635 c -induced apoptosis pathway: absolute requirement for removal of caspase-6  
636 prodomain. *Cell Death Differ.* 2002 Oct;9(10):1046–56.

637 42. Spencer SL, Gaudet S, Albeck JG, Burke JM, Sorger PK. Non-genetic origins of cell-to-cell  
638 variability in TRAIL-induced apoptosis. *Nature.* 2009 May;459(7245):428–32.

639 43. Skilling J. Nested sampling for general Bayesian computation. *Bayesian Anal.* 2006  
640 Dec;1(4):833–59.

641 44. Feroz F, Hobson MP, Bridges M. MultiNest: an efficient and robust Bayesian inference  
642 tool for cosmology and particle physics. *Mon Not R Astron Soc.* 2009 Oct 1;398(4):1601–  
643 14.

644 45. Feroz F, Hobson MP, Cameron E, Pettitt AN. Importance Nested Sampling and the  
645 MultiNest Algorithm. *arXiv:13062144 [astro-ph, physics:physics, stat] [Internet].* 2013 Jun  
646 10 [cited 2019 May 14]; Available from: <http://arxiv.org/abs/1306.2144>

647 46. Buchner J, Georgakakis A, Nandra K, Hsu L, Rangel C, Brightman M, et al. X-ray spectral  
648 modelling of the AGN obscuring region in the CDFS: Bayesian model selection and  
649 catalogue. *A&A.* 2014 Apr 1;564:A125.

650 47. Burnham KP, Anderson DR. *Model Selection and Multimodel Inference: A Practical  
651 Information-Theoretic Approach [Internet].* 2nd ed. New York: Springer-Verlag; 2002  
652 [cited 2019 Apr 24]. Available from: <https://www.springer.com/us/book/9780387953649>

653 48. Symonds MRE, Moussalli A. A brief guide to model selection, multimodel inference and  
654 model averaging in behavioural ecology using Akaike's information criterion. *Behav Ecol  
655 Sociobiol.* 2011 Jan 1;65(1):13–21.

656 49. Shockley EM, Rouzer CA, Marnett LJ, Deeds EJ, Lopez CF. Signal integration and  
657 information transfer in an allosterically regulated network. *npj Syst Biol Appl.* 2019 Jul  
658 18;5(1):1–9.

659 50. Dai H, Ding H, Peterson KL, Meng XW, Schneider PA, Knorr KLB, et al. Measurement of  
660 BH3-only protein tolerance. *Cell Death and Differentiation.* 2018 Jan 1;25(2):282–93.

661 51. Eissing T, Conzelmann H, Gilles ED, Allgöwer F, Bullinger E, Scheurich P. Bistability  
662 Analyses of a Caspase Activation Model for Receptor-induced Apoptosis. *J Biol Chem.*  
663 2004 Aug 27;279(35):36892–7.

664 52. Eydgahi H, Chen WW, Muhlich JL, Vitkup D, Tsitsiklis JN, Sorger PK. Properties of cell  
665 death models calibrated and compared using Bayesian approaches. *Molecular Systems  
666 Biology.* 2013 Jan 1;9(1):644.

667

668 53. Aitken S, Akman OE. Nested sampling for parameter inference in systems biology:  
669 application to an exemplar circadian model. *BMC Systems Biology*. 2013 Jul 30;7(1):72.

670 54. Pullen N, Morris RJ. Bayesian Model Comparison and Parameter Inference in Systems  
671 Biology Using Nested Sampling. *PLOS ONE*. 2014 Feb 11;9(2):e88419.

672 55. Xu T-R, Vyshevirskey V, Gormand A, Kriegsheim A von, Girolami M, Baillie GS, et al.  
673 Inferring Signaling Pathway Topologies from Multiple Perturbation Measurements of  
674 Specific Biochemical Species. *Sci Signal*. 2010 Mar 16;3(113):ra20–ra20.

675 56. MacKay DJC, Kay DJCM. *Information Theory, Inference and Learning Algorithms*.  
676 Cambridge University Press; 2003. 696 p.

677 57. Certo M, Moore VDG, Nishino M, Wei G, Korsmeyer S, Armstrong SA, et al. Mitochondria  
678 primed by death signals determine cellular addiction to antiapoptotic BCL-2 family  
679 members. *Cancer Cell*. 2006 May 1;9(5):351–65.

680 58. Burnham KP, Anderson DR. *Model Selection and Multimodel Inference: A Practical  
681 Information-Theoretic Approach [Internet]*. 2nd ed. New York: Springer-Verlag; 2002  
682 [cited 2019 Oct 26]. Available from: <https://www.springer.com/gp/book/9780387953649>

683 59. Symonds MRE, Moussalli A. A brief guide to model selection, multimodel inference and  
684 model averaging in behavioural ecology using Akaike's information criterion. *Behav Ecol  
685 Sociobiol*. 2011 Jan 1;65(1):13–21.

686 60. Aldridge BB, Gaudet S, Lauffenburger DA, Sorger PK. Lyapunov exponents and phase  
687 diagrams reveal multi-factorial control over TRAIL-induced apoptosis. *Molecular Systems  
688 Biology*. 2011 Jan 1;7(1):553.

689 61. Handley WJ, Hobson MP, Lasenby AN. PolyChord: next-generation nested sampling. *Mon  
690 Not R Astron Soc*. 2015 Nov 11;453(4):4385–99.

691 **Supporting information**

692 Table S1

693 Table S2

694 Table S3

695 Table S4

696 Table S5

697 Table S6

698 Figures S1-S4

699

700 **Figures Legends:**

701 **Figure 1. General workflow for the analysis of network dynamics using trends in Bayesian evidence.** The target  
702 network is first deconstructed into all relevant subnetworks. A model for each subnetwork and each incrementing  
703 set of regulatory conditions is then created and passed to an algorithm for estimation the Bayesian model  
704 evidence. The evidence is calculated on a user-defined objective function, describing signal transduction through  
705 the network, and over a range of parameter values (the prior). The evidence trends over changing regulatory  
706 conditions are then compared to make qualitative inferences regarding network dynamics. In an alternative  
707 method, the full model is retained, but the objective function is targeted to different pathways. Inferences on  
708 network dynamics can again be made from the trends in the evidence calculations.

709

710 **Figure 2. Extrinsic apoptosis subnetworks and Bayesian evidence for achieving apoptosis.** (A) The direct caspase  
711 subnetwork. (B) The direct caspase + mitochondrial activation subnetwork. (C) The direct caspase + mitochondrial  
712 inhibition of XIAP subnetwork network. (D) The mitochondrial activation subnetwork. (E) The complete network.  
713 (F) the mitochondrial subnetwork. (G) The trends in Bayesian evidence for each of the networks in (A)-(F) over a  
714 range of values the apoptosis inhibitor XIAP and for an objective function that computes the proportion of PARP  
715 cleavage (a proxy for cell death) at the end of a simulated run.

716

717 **Figure 3. Evidence values for PARP cleavage and pathway flux at low and high DISC values.** (A) Evidence values  
718 for PARP cleavage for the caspase pathway and complete network under both low and high DISC conditions (100  
719 and 130,000 molecules per cell of FADD and Caspase-8 respectively). (B) Signal flux through both pathways as well  
720 as the total signal flux for high DISC values. (C) Signal flux through both pathways as well as the total signal flux for  
721 low DISC values.

722

723 **Figure 4. Evidence ratio trends under increasing levels of the apoptotic inhibitor XIAP for an inhibited and  
724 uninhibited mitochondrial pathway.** (A) Evidence trends for the caspase pathway (green), mitochondrial pathway  
725 (blue), and complete network (orange) with no MOMP inhibition. (B) Trends for the mitochondria/caspase (blue)  
726 and the complete/caspase (orange) evidence ratios from the trends in (A). (C) Evidence trends for the caspase  
727 pathway (green), mitochondrial pathway (blue), and complete network (orange) with MOMP inhibitory protein  
728 BCL-2 at 328,000 mol. per cell. (D) Trends for the mitochondria/caspase (blue) and the complete/caspase (orange)  
729 evidence ratios from the trends in (C).

730

731 **Figure 5. Precision vs. computational cost.** (A) and (B) Average number of evaluations before termination of the  
732 MultiNest algorithm over a range of population sizes for the caspase pathway and complete network respectively.  
733 (C) and (D) Average of error estimates from MultiNest for each population size and the caspase and complete  
734 networks. (E) and (F) Average estimated CPU clock time over each population size for the caspase and complete  
735 networks respectively. \*MultiNest was unable to estimate the error at XIAP = 0.

736

737

738 **Box 1. Extrinsic apoptosis execution.**

739 Extrinsic apoptosis is a receptor mediated process for programmed cell death. The Type I/II phenotypes for the  
740 extrinsic apoptosis system were first described by Scaffidi et al. [13]. In that work they examined several cell lines  
741 and classified them into those that required the mitochondrial pathway to achieve apoptosis (Type II) and those  
742 that don't (Type I). They made several interesting conclusions. They found that Type II cells had relatively weak  
743 DISC formation, that both phenotypes responded equally well to receptor mediated cell death, that there was a  
744 delay in caspase activation in Type II cells, and that caspase activation happened upstream of mitochondrial  
745 activation in Type I cells and downstream in Type II. More recently, XIAP has also been put forth as a critical  
746 regulator in the choice of apoptotic phenotype. In Jost et al. [14] they examined hepatocytes (Type II cells) and  
747 lymphocytes (Type I cells) under different conditions to examine the role XIAP plays in Type I/II determination.  
748 They made several observations upon Fas ligand or Fas-antibody induced apoptosis such as higher levels of XIAP in  
749 Type II cells and higher caspase effector activity in XIAP/Bid deficient mice versus apoptosis resistant Bid-only  
750 knockouts. In all, they concluded that XIAP is the key regulator that determines the choice of pathway.

751 Extrinsic apoptosis is initiated when a death inducing member of the tumor necrosis factor (TNF) superfamily of  
752 receptors (FasR, TNFR1, etc.) is bound by its respective ligand (FasL, TNF- $\alpha$ , etc.), setting off a sequence  
753 biochemical events that result in the orderly deconstruction of the cell [15]. The first stage of this sequence is the  
754 assembly of the DISC at the cell membrane ① and the subsequent activation of Caspase-8. Upon ligand binding  
755 and oligomerization of a receptor such as FasR or TRAIL, an adapter protein, like FADD (Fas-associated protein with  
756 death domain), is recruited to the receptors cytoplasmic tail [16, 17, 18]. FADD, in turn, recruits Caspase-8 via their  
757 respective death effector domains (DEDs), thus completing DISC formation [17, 18]. Other DISC components could  
758 also be included here, such as the regulator cFlip [19]. Once recruited, proximal ProCaspase-8 monomers dimerize,  
759 inducing their autoproteolytic activity and producing active Caspase-8 [20, 21, 22].

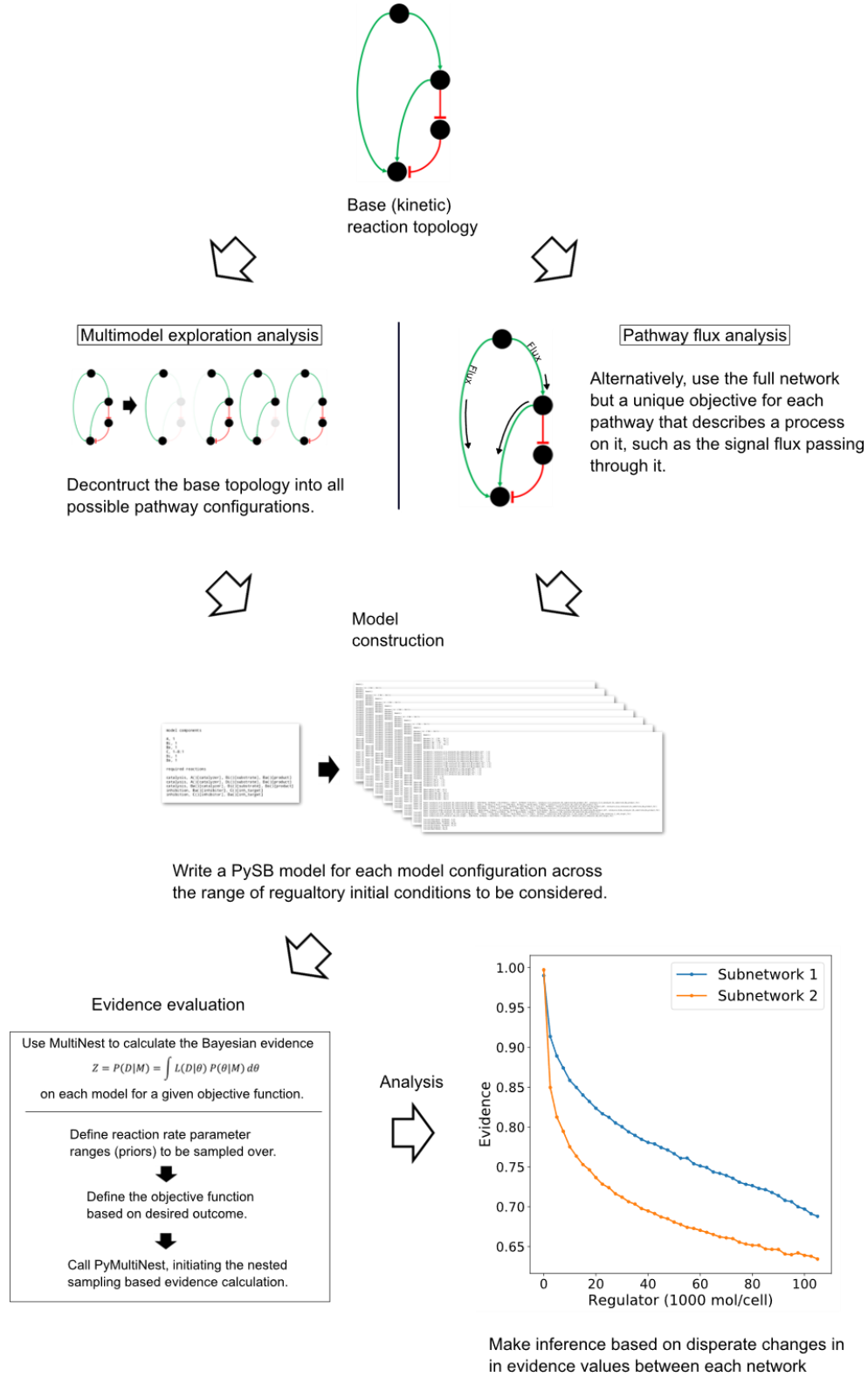
760 After Caspase-8 activation the apoptotic signal can progress down two distinct pathways that both lead to the  
761 activation of Caspase-3 and the ensuing proteolysis of downstream targets. One pathway consists of a caspase  
762 cascade in which active Caspase-8 directly cleaves and activates Caspase-3 ② [23], while another, more complex  
763 pathway is routed through the mitochondria. In the mitochondrial pathway Caspase-8 cleaves the pro-apoptotic  
764 Bcl-2 family protein Bid in the cytosol, which then migrates to the mitochondria ③ where it initiates  
765 mitochondrial outer membrane permeabilization (MOMP) and the release of pro-apoptotic factors that lead to  
766 Caspase-3 activation [24, 25].

767 MOMP has its own set of regulators that govern the strength of apoptotic signaling through the mitochondria ④.  
768 After Caspase-8 activated Bid, (tBid), migrates to the mitochondria it activates proteins in the outer mitochondrial  
769 membrane, such as Bax, that subsequently self-aggregate into membrane pores and allow exportation of  
770 Cytochrome-c and Smac/DIABLO to the cytosol [26]. Bid and Bax are examples of pro-apoptotic proteins from the  
771 Bcl-2 family, all of which share BH domain homology [27]. Other members of this family act as MOMP regulators;  
772 the anti-apoptotic Bcl-2, for example, binds and inhibits both Bid and Bax while the pro-apoptotic Bad similarly  
773 binds and inhibits its target, Bcl-2 [28, 29, 30, 31]. Many other pro- and anti-apoptotic members of the Bcl-2 family  
774 have been discovered and together regulate MOMP [32].

775 Regardless of which pathway is chosen, the intermediate results are Caspase-3 activation and subsequent cleavage  
776 of PARP ⑧, a proxy for cell death in the analyses here [33, 34]. XIAP (X-linked inhibitor of apoptosis protein) is an  
777 inhibitor of Caspase-3 and has been proposed to be a key regulator in determining the Type I/II apoptotic  
778 phenotype of a cell [35]. XIAP sequesters Caspase-3 but also contains a ubiquitin ligase domain that directly targets  
779 Caspase-3 for degradation. The inhibitor also sequesters and inhibits the Caspase-3 activating Caspase-9 residing  
780 within the apoptosome complex [36, 37, 38]. Apoptosome formation is initiated by Cytochrome-c exported from  
781 the mitochondria during MOMP ⑤. Cytochrome-c induces the protein APAF-1 to oligomerize and subsequently  
782 recruit and activate Caspase-9, thus forming the complex [39]. Another MOMP export, the protein Smac/DIABLO  
783 ⑥, binds and inhibits XIAP, working in tandem with Cytochrome-c to oppose XIAP and carry out the apoptosis  
784 inducing activity of the Type II pathway [40]. Finally, ProCaspase/Caspase-6 constitutes a feed forward loop  
785 between Caspase-3 and Caspase-8 ⑦ [41].

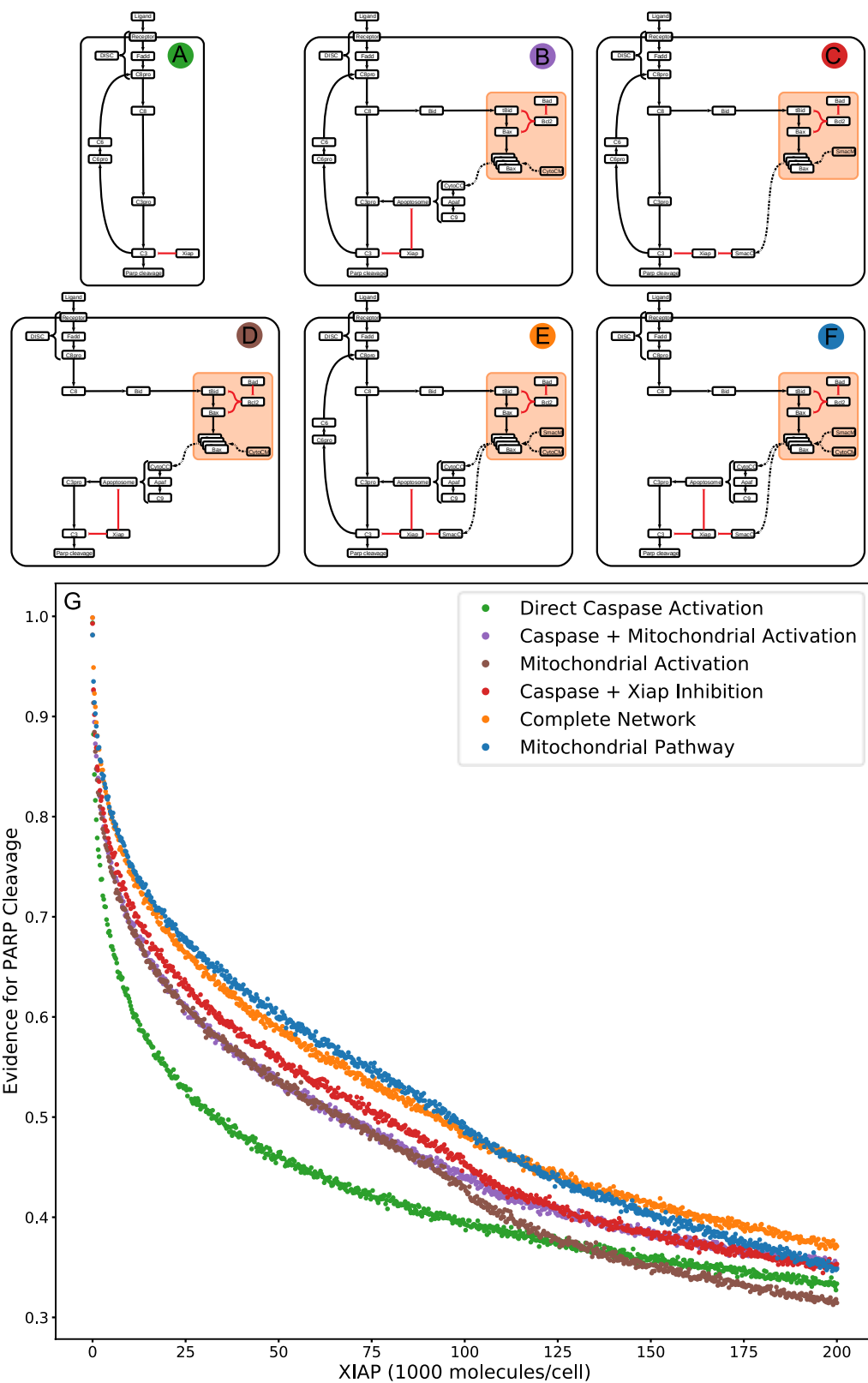
786

787 **Figures:**  
788 **Figure 1.**



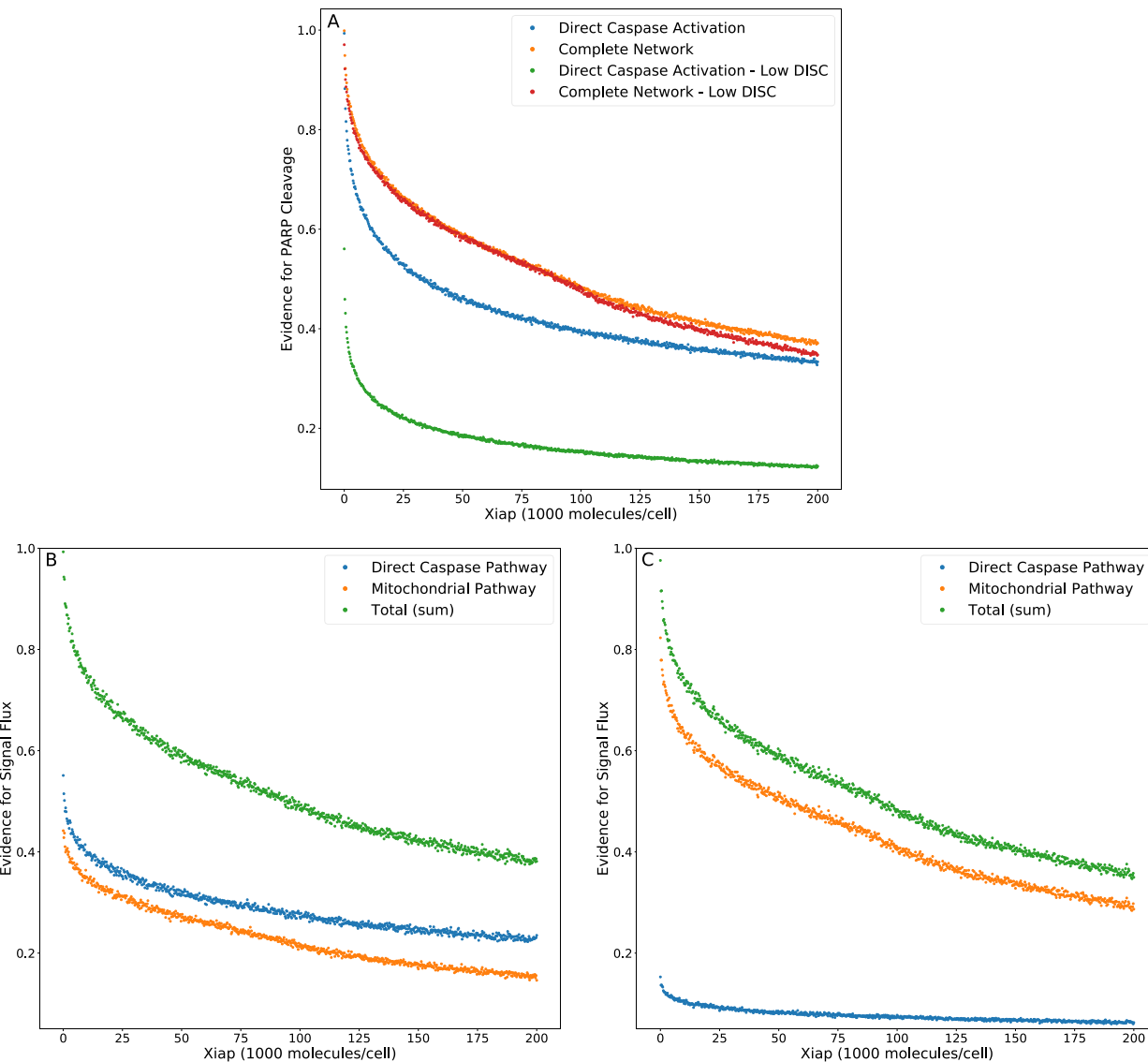
789

790 **Figure 2.**



791

792 **Figure 3.**



793

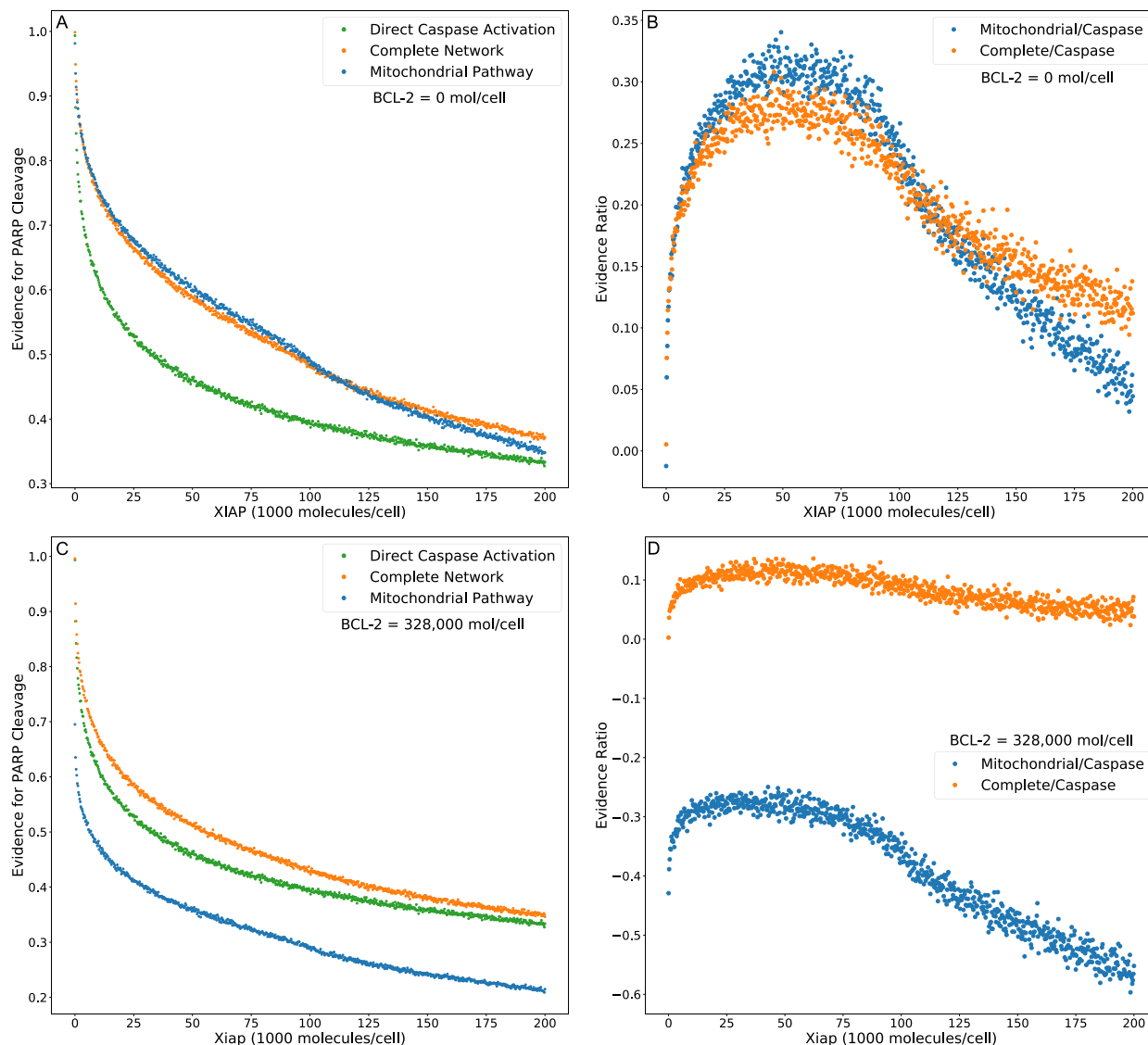
794

795

796

797

798 **Figure 4.**



799

800

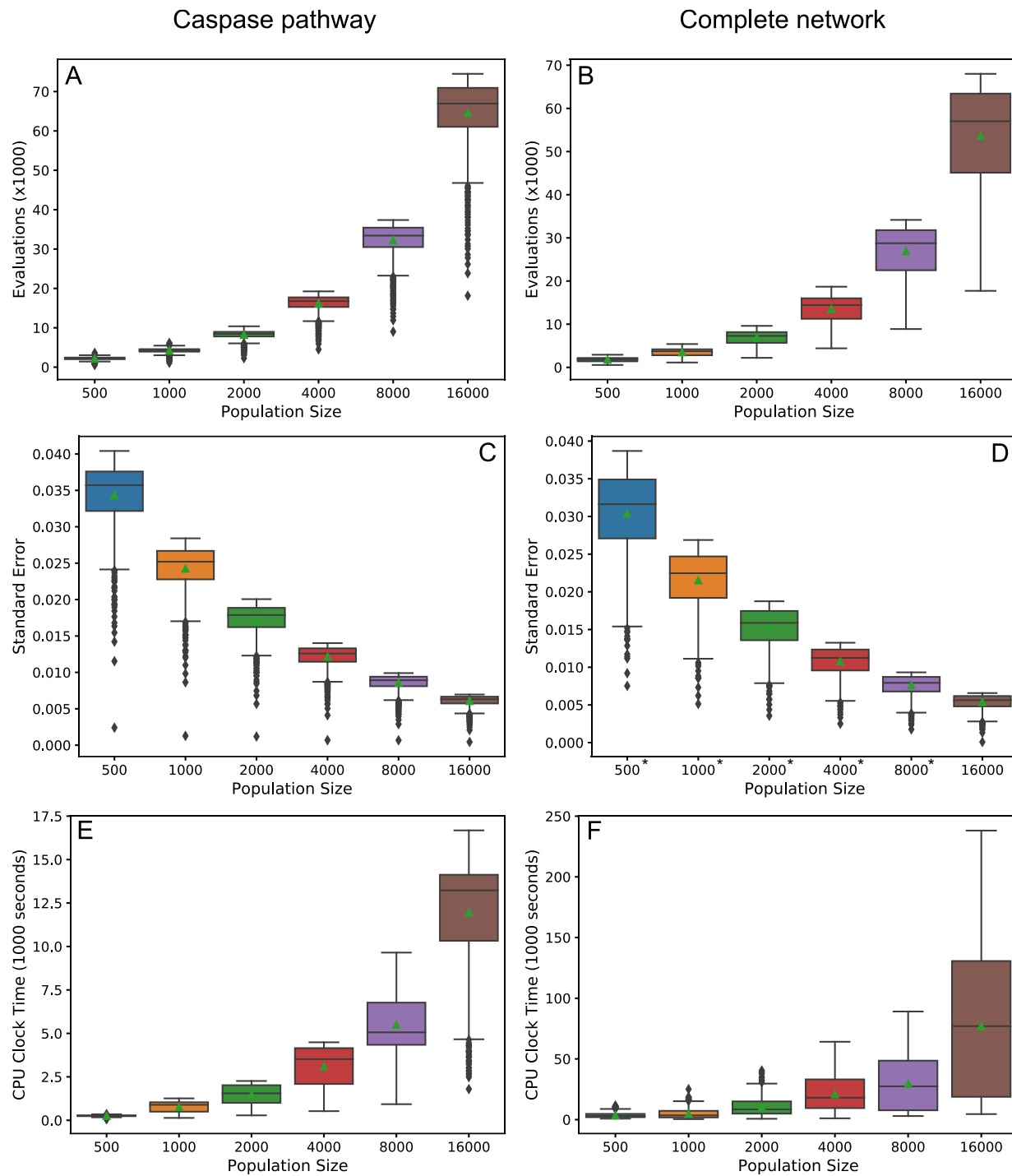
801

802

803

804

805 **Figure 5.**



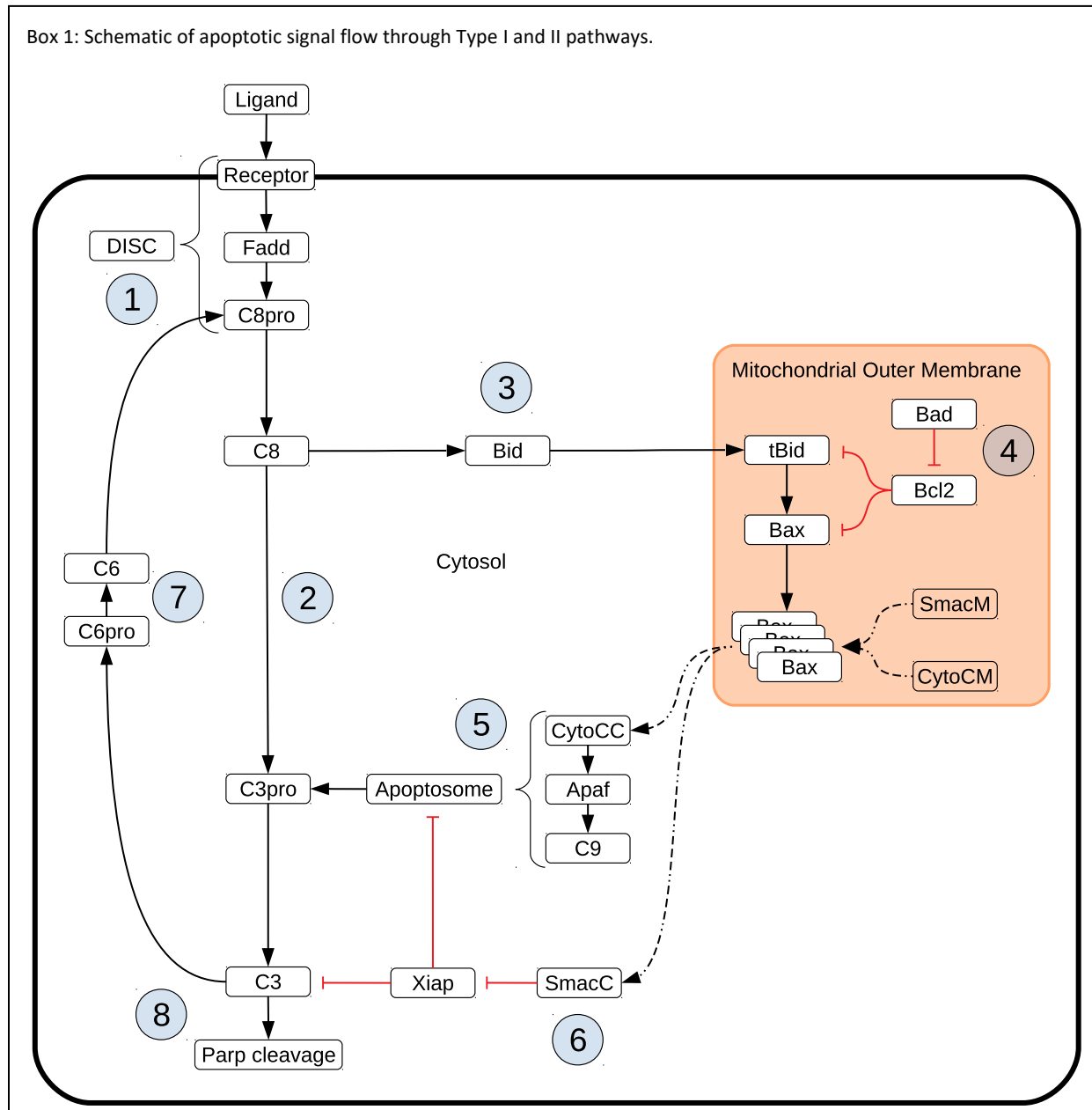
806

807

808

809

810 **Box 1.**



811

812